Cellulose (2020) 27:335–345
https://doi.org/10.1007/s10570-019-02761-x

ORIGINAL RESEARCH

Regenerated cellulose-based composite membranes as adsorbent for protein adsorption

Qi Zhou · Yuping Bao · Hao Zhang · Qian Luan · Hu Tang · Xiuting Li

Received: 24 July 2019 / Accepted: 18 September 2019 / Published online: 9 October 2019

Abstract The development of protein adsorbents with high adsorption performance has attracted great attention due to the important role of these adsorbents in protein separation and purification. Herein, cellulose-based composite membranes were prepared through a combination of cellulose fiber (CF) and 2,2,6,6-tetramethylpiperidine-1-oxyl oxidized cellulose nanofiber (CNF) in alkaline/urea aqueous solution and regeneration from a tape casting method. Taking advantage of the functional carboxyl groups in CNF, the obtained cellulose-based composite membranes display a good protein adsorption property, with a capacity of 241.6 mg g^{-1}, by using bovine serum albumin as a model protein. Meanwhile, the adsorption performance of cellulose-based composite membranes can be optimized by regulating the blending ratios of CNF and CF, buffer pH, initial protein concentrations and temperature, and the mechanical property of cellulose-based composite membranes can be adjusted by changing the ratio of CNF and CF. These effective and economic membranes may act as promising candidates for protein adsorption in protein separation and purification fields.

Keywords Cellulose nanofiber · Cellulose fiber · Membrane · Protein adsorption

Qi Zhou and Yuping Bao have contributed equally to this work and co-first authors.

Electronic supplementary material The online version of this article (https://doi.org/10.1007/s10570-019-02761-x) contains supplementary material, which is available to authorized users.

Q. Zhou · H. Tang · X. Li (✉)
Beijing Advanced Innovation Center for Food Nutrition and Human Health, Beijing Technology and Business University, Beijing 100048, China
e-mail: lixt@th.btbu.edu.cn

Q. Zhou · Y. Bao · H. Zhang · Q. Luan · H. Tang (✉)
Key Laboratory of Oilseeds Processing, Ministry of Agriculture, Hubei Key Laboratory of Lipid Chemistry and Nutrition, Oil Crops and Lipids Process Technology National and Local Joint Engineering Laboratory, Oil Crops Research Institute, Chinese Academy of Agricultural Sciences, Wuhan 430062, China
e-mail: th725@163.com

Introduction

Interest in the development of protein adsorbents has been increasing owing to the widespread applications of pharmaceutical protein products in fields such as disease diagnosis, prevention, and treatment (Fu et al. 2016; Handschuh-Wang et al. 2016; Richter and Ivan 2013). Controllable attachment of biomolecules is an essential ability for functional materials to play roles in diagnostic and medical applications (Hazarika et al. 2014).

Cellulose, a liner homopolymer of cellobiose units connected by β-(1 − 4) glycosidic bonds with

nontoxic, biodegradable, economic and easy derivative properties, has been attested by previous researchers as particularly friendly of protein and biomolecule (Duan et al. 2015; Pelton 2009). Cellulose membranes have been widely used for pervaporation (Dubey et al. 2005), ultrafiltration (Madaeni and Heidary 2011) and protein adsorption (Fu et al. 2018) because of the biocompatibility, large specific surface area, porous structure, and good mechanical property (Hu et al. 2011). However, the adsorption performance of the cellulose membranes would be low with weak interaction between the adsorbent and biomolecule (Hao et al. 2018). Researches have shown that charged membranes can perform well during protein adsorption and separation process because of their pH controllability and special anti-fouling potential (Zhao et al. 2003). Physical blends (Hao et al. 2018) and chemical modification (Sahadevan et al. 2018) have been widely used for the functionalization of cellulose membranes to endow them with unique functional properties. Hao et al. (2018) has developed cellulose-based protein adsorbent through the combination of cellulose membranes with functional magnetite nanoparticles, the active amino groups and carboxyl groups on magnetite nanoparticles have endowed the composite membranes with controllable protein adsorption performance. Sahadevan et al. (2018) has developed cellulose-graft-polyethyleneamidoamine nanofiber membrane absorbent through redox polymerization, which could perform effective separation for biomolecules, but the fabrication process is complex.

Common cellulose derivatives such as carboxymethyl cellulose or hydroxypropyl cellulose are usually not substituted equally, and the cellulose derivatives are water soluble so as to limit their applications (Bhatt et al. 2011; Kamide et al. 1985; Luan et al. 2017). Especially, TEMPO-oxidation could effectively introduce large amounts of carboxylic groups into cellulose fiber by exclusively converting primary C6-OH groups to carboxylic moieties (Tsuguyuki et al. 2007). The abundant carboxyl groups could provide the cellulose-based membranes with charged properties to use for protein adsorption.

In this study, we demonstrate the fabrication of a protein adsorbent based on TEMPO-oxidized cellulose nanofiber (CNF) and cellulose fiber (CF). The combination of abundant carboxyl groups on CNF and good mechanical properties of CF could be an effective and simple pathway for the construction of protein adsorbent. CNF was first prepared by an oxidization of cellulose fiber using TEMPO, then cellulose-based composite membranes were obtained by a combined dissolution of CNF and CF in alkaline/urea aqueous solution and regeneration from a tape casting method. Benefiting from the unique properties such as the abundant hydroxyl groups and carboxyl groups, large specific surface area, and porous structure, the resultant cellulose-based composite membrane exhibit good performance in protein adsorption.

Experimental

Materials

Cotton linter pulp contains more than 95% of α-cellulose was obtained from Hubei Chemical Fiber Co. Ltd. (Xiangyang, China). The viscosity-average molecular weight (M_v), measured according to a previous research of Cai et al. was 1.0×10^5 g mol^{-1} (Jie and Lina 2006). TEMPO, sodium hypochlorite (NaClO), sodium bromide (NaBr), and bovine serum albumin (BSA, biotechnological grade, purity > 96%) were obtained from Sigma-Aldrich (United States). BCA Protein Assay Kit was from Nanjing Jiancheng Bioengineering Institute (Nanjing, China). Other chemicals of analytical grade were provided by Sinopharm Chemical Reagent Co., Ltd. (China).

Preparation of cellulose nanofiber

Cotton linter pulp was modified by a TEMPO oxidation system according to a previous research of Tsuguyuki et al. (2007). Generally, 1 wt% cotton linter pulp suspension was prepared in advance by dispersing cotton linter pulp into deionized water. TEMPO (0.016 wt% of the suspension) and NaBr (0.1 wt% of the suspension) were then added and stirred for 0.5 h. The pH of the suspension was adjusted and maintained at 10 ± 0.1 by adding NaClO with constant mechanical stirring (380 rpm), and 0.1 M NaOH solutions were further used after the consumption of NaClO (0.075 mmol g^{-1} of the suspension). The experiment was finished when the pH of the suspension changed no more, and the obtained suspension was washed by dialyzing

thoroughly against deionized water. Finally, the obtained cellulose nanofiber (CNF) was stored in a fridge (4 °C) for further application.

Preparation of cellulose-based composite membranes

CF and CNF solutions were first prepared by dissolution of 8 g CF and 16 g CNF in 200 g aqueous LiOH/urea/water (8/15/77) solution using a freezing/thawing method, respectively (Meng et al. 2012). CF and CNF solutions were mixed and stirred to get homogeneous cellulose composite solutions. The obtained solution were centrifuged at 5322 g for 15 min using a centrifuge (Avantj J-25, Beckman) to obtain a transparent solution. Cellulose-based composite membranes were then prepared by using a tape casting method according to a previous research (Meng et al. 2012). Briefly, the above transparent solution was cast on a glass plate and followed by immersion into a coagulating bath (5 wt% H_2SO_4/10 wt% Na_2SO_4 aqueous solution) immediately for coagulation and regeneration. The obtained membranes were rinsed with pure water until the washings were neutral and stored at 4 °C. A series of composite membranes were obtained by adjusting the blending ratio of CNF and CF (2:1, 1:1, and 1:2), and these membranes were coded as CNCM21, CNCM11, and CNCM12, whereas pure CNF and CF regenerated membranes were coded as CNM, CM, respectively.

Characterization

The carboxylate content of CNF, measured according to a conductometric titration method (Montanari et al. 2008), was 1.43 mmol g^{-1} (Fig. S1, Table S1). For scanning electron microscopy (SEM) observation, wet membranes were frozen using liquid nitrogen, snapped, freeze-dried, and sputtered with gold. SEM images were then obtained by a Hitachi SU8010 (Tokyo, Japan) microscope. Fourier-transform infrared spectroscopy (FT-IR) was performed on PerkinElmer 1600 (USA). X-ray diffraction (XRD) analysis was conducted on Rigaku Denki D/MAX-1200 (Japan) in the scanning range of 5°–40° at a speed of 5° min^{-1} with Cu Kα radiation at 40 kV and 30 mA. The samples were cut into pieces and dried at 60° overnight for FTIR and XRD analyses. The mechanical properties of membranes in the dry and wet states were measured by using CMT6503 (SANS TEST machine, China) (Hu et al. 2011) at the speed of 1 mm min^{-1} and 5 mm min^{-1}, respectively. The tests of each sample were repeated for five times to obtain an average value.

Swelling behavior

The swelling studies of CNM, CNCM21, CNCM11, CNCM12, and CM were carried out according to a previous research (Doulabi et al. 2013). Freeze-dried samples with size of 2 cm × 2 cm were immersed into 0.1 M pH 7.4 phosphate buffered saline (PBS) solution and swollen at 37 °C. The samples were weighed and recorded as W_w after 24 h of immersion and gently blotted with filter paper. The samples were then dried and weighed (W_d). The Swelling ratio (SR) was calculated using the following equation:

$$\mathrm{SR}\,(\%) = \frac{w_w - w_d}{w_d} \times 100\% \quad (1)$$

The measurement of the swelling ratio of each sample was repeated for three times.

Point of zero charge

Point of zero charge (pzc) is the media solution pH at which the net surface charge of test sample is zero, and the pzc of composite membranes was measured as it is closely related to the phenomenon of adsorption (Marek 2014; Udoetok et al. 2016). Briefly, 8 beakers with 20 mL NaCl solution (0.05 M) in each were prepared. The pH of the solution was adjusted from 1 to 8 by using 0.1 M HCl or NaOH solutions, the volume of the solution in each beaker was increased to 30 mL by the addition of NaCl solution, and the pH of the solution was recorded (pH_i). Then, the composite membranes were immersed in each of the solution and shaken at 90 rpm (HYL-C, Taicang Qiangle experimental equipment Ltd., china, 25° ± 2°). The membranes were taken out after 48 h and the pH of the solution was recorded (pH_f). The pzc was obtained from the plot of ΔpH (pH_i–pH_f) versus pH_i.

BSA adsorption experiments

To determine the optimized pH of absorption, the effects of pH on BSA adsorption capacities of the composite membranes were evaluated. 25 mg samples

were immersed into 25 mL 200 mg L^{-1} BSA solutions within the flasks in the pH range of 4.0, 4.5, 5.0 and 6.0, respectively. The flasks were then shaken at 25 °C under 90 rpm for 24 h. The concentrations of BSA before and after adsorption were measured by SpectraMax spectrophotometer (M2e) at a wavelength of 562 nm using BCA protein assay kit (Yang et al. 2013). The amount of adsorbed BSA (q_e) was calculated using Eq. (2):

$$q_e = \frac{C_0 - C_e}{m} \times V \quad (2)$$

where C_o (mg L^{-1}) and C_e (mg L^{-1}) are the BSA concentration of solution before and after adsorption, respectively, V (L) is the volume of solution, and m (g) is the weight of the composite membranes.

To evaluate the effect of initial protein concentration, 25 mg samples were added into 25 mL BSA solution (the pH optimized as 4.5 according to the above experiments) with concentration ranging from 50 to 4000 mg L^{-1}. The experiments were performed at 288, 298, and 308 K, respectively. The mean values were obtained through three times repeated experiments.

Results and discussion

Morphology of cellulose-based composite membranes

SEM was used for the observation of the morphological properties of the composite membranes (Fig. 1). The membranes display homogeneous microporous structures, suggesting the good miscibility of CNF and CF within the composite membranes. It is also observed that the structures change with the adjustment of CF/CNF ratios in the composite membranes. These composite membranes were further analyzed using ImageJ software to study the pore size distribution and the results are shown in the right side of Fig. 1 (Sadir et al. 2014). CNM has the largest average pore size (1.31 μm) in comparison with the other composite membranes, and the average pore size was found decrease to 0.69 μm from CNM to CM. This could be explained by the decrease of CNF content, which leads to the decrease of carboxylate contents, and the carboxylate contents might contribute to the formation of pores during the regenerated process of composite membranes (Zhang et al. 2017). The results of SEM and pore size analysis suggest the adjustment of the blending ratio of CNF and CF can have a direct effect on the carboxyl group contents and porous structure of the composite membranes, which is helpful for the fabrication of adsorbent with controllable functional groups and pore size.

Structural characterization of cellulose-based composite membranes

The chemical structural variations were recorded using FTIR spectroscopy (Fig. 2). The successful modification of CF was evident from the band at 1618 cm^{-1} in the spectrum of CNF, which is ascribed to carboxyl groups in salt form (COO^-) (Zhang et al. 2018). The abundant carboxyl groups within the composite membranes would thus be beneficial for protein adsorption. Compared with CF and CNF, the band around 895 cm^{-1} owing to the stretching vibration of ν(C–O–C) at the β-(1-4)-glycosidic linkage increased apparently in the spectrum of the regenerated membranes, and the band at 1282 cm^{-1} due to δ(C–H) shifted to lower wave number (Dinand et al. 2002; Sang et al. 2005). These results indicate the dissolution and regeneration process can lead to the cellulose I structure changes to cellulose II (Luo et al. 2009). The intensity of ν(C=O) stretching bands at 1735 cm^{-1} was gradually decreased with the decrease of CNF content from Fig. 2c–g owing to the reduced amount of carboxyl groups, indicate the simple method of controlling the absorption sites within the composite membranes.

To better understand the chemical structural features of the composite membranes, the crystalline structure was evaluated. In Fig. 3a, the peaks at 2θ = 14.9°, 16.6°, 22.8°, and 34.5° were ascribed to cellulose I structure (Chang et al. 2008). These were also found in CNF and thus can be attributed to the fact that the introduced carboxyl groups only exist on surfaces of CNF (Luan et al. 2017). With respect to the composite membranes (Fig. 3c–g), the peaks at 2θ = 12.1°, 19.8°, and 22.6° corresponding to cellulose II structure (Sang et al. 2005). The result is in agreement with FTIR results, indicated that the cellulose I crystal structure was changed to cellulose II in the process of dissolution and regeneration.

The mechanical property is one of the key functions of the composite membrane for industrial application

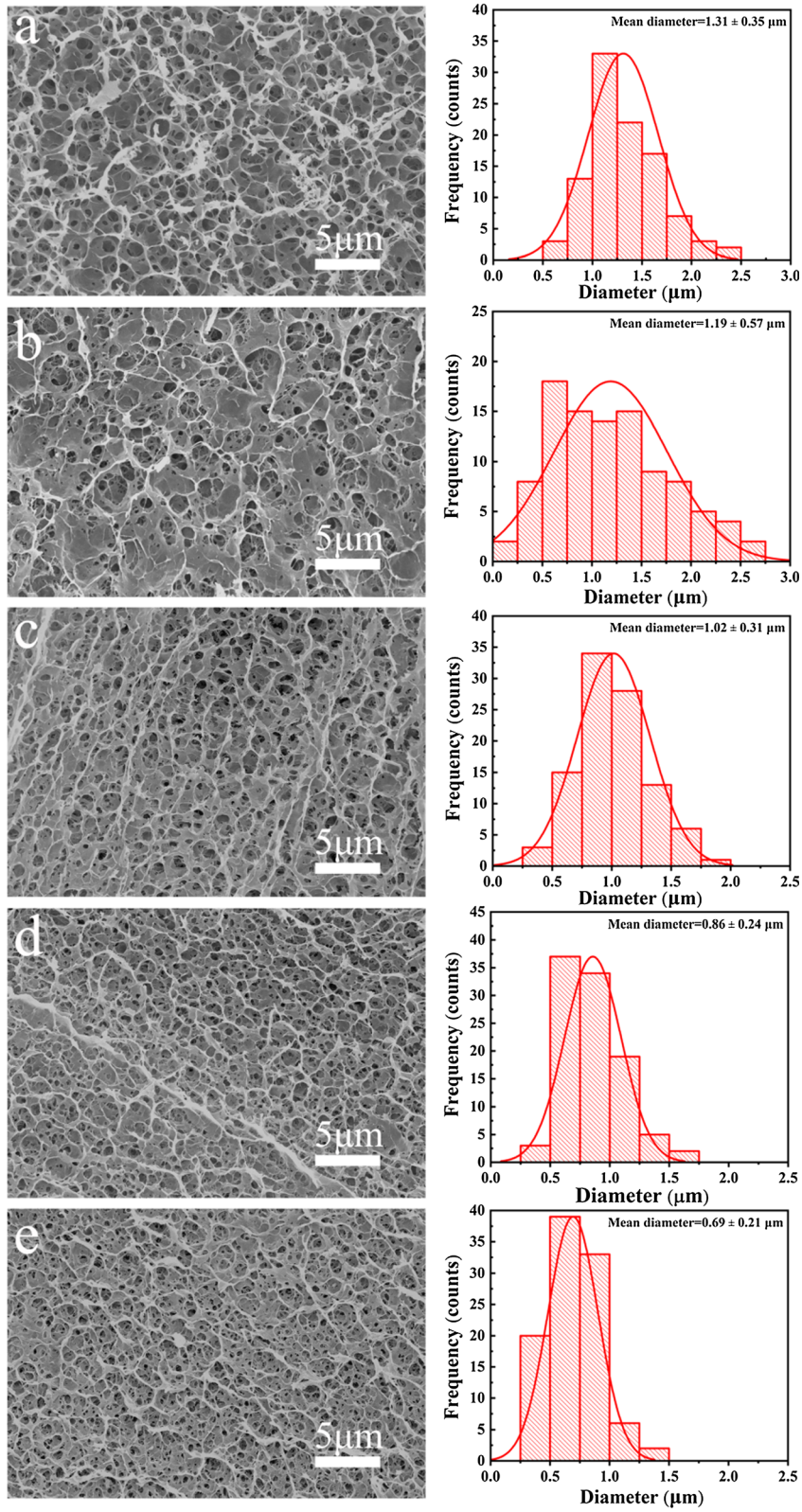

Fig. 1 SEM images and pore size distributions of CNM (**a**), CNCM21 (**b**), CNCM11 (**c**), CNCM12 (**d**), CM (**e**)

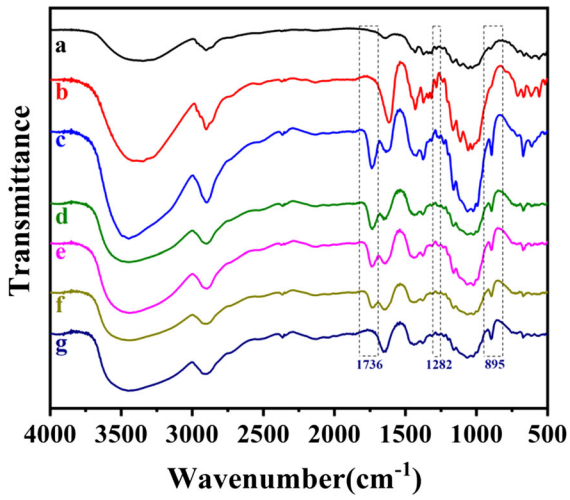

Fig. 2 FT-IR spectra of CF (a), CNF (b), CNM (c), CNCM21 (d), CNCM11 (e), CNCM12 (f), CM (g)

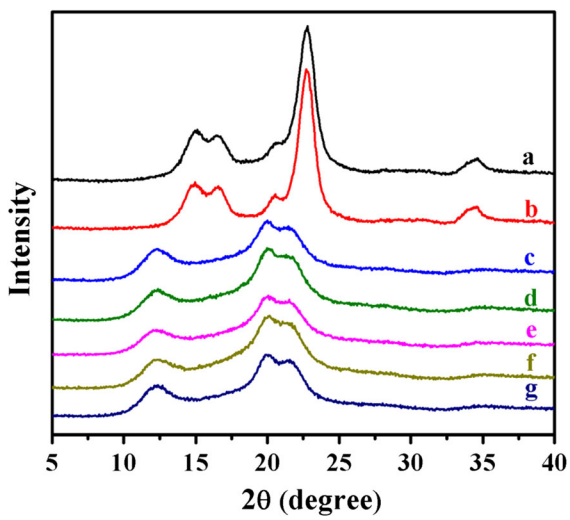

Fig. 3 XRD patterns of CF (a), CNF (b), CNM (c), CNCM21 (d), CNCM11 (e), CNCM12 (f), CM (g)

as protein adsorbent. The effects of CF/CNF ratios on mechanical properties were investigated by using tensile tests. It was observed from Fig. 4 and Table 1 that the tensile strength and elongation at break of the membranes in both states were increased with increasing content of CF. The tensile strength of the CNM was noted at 17.78 ± 1.09 MPa, whereas it was observed at 86.05 ± 0.36 MPa for CNCM12. Elongation at break of CNM and CNCM12, presents the same trend as the tensile strength, were 0.99 ± 0.07% and 4.20 ± 0.07% at dry state, respectively. The tensile tests suggest that the adjustment of CNF/CF ratios within the composite membranes can directly affect the mechanical properties.

Swelling behavior

The water absorption capacity of the membrane absorbents has an effect on the interaction process between protein and the membranes (Abedini 2011). Thus, the swelling behaviors of the composite membranes were determined and the results were shown in Fig. 5. The swelling ratios of CNM, CNCM21, CNCM11, CNCM12 and CM, gradually decreased with increasing CF contents, were 158.0 ± 4.36%, 127.3 ± 2.08%, 111.3 ± 1.53%, 95.3 ± 1.53%, and 78.7 ± 2.52%, respectively. These results could be owing to the function of hydrophilic COO^- groups in the composite membranes, and the decrease of CNF and increase of CF result in the decrease of carboxyl groups in the composites (Zhang et al. 2017).

BSA adsorption experiments

Effect of pH

The effect of pH on BSA adsorption was investigated to determine the optimized pH of absorption as the pH of protein solution has a close relationship with the protein absorption. It is observed from Fig. 6 that all of the composite membranes display pH-dependent adsorption behaviors. At pH 4.5, all of the samples could absorb the highest amount of BSA. The adsorption performance was gradually increased from CM to CNM at pH 4.0 and 4.5. On the contrary, CM displayed the highest adsorption capacity at pH 6.0 among these composite membranes, and the adsorption capacity was gradually decreased from CM to CNM. These interesting phenomena were resulted from the changes of the surface charge of the membranes and BSA at different pH. It is known from previous research that the isoelectric point of BSA is 4.7, and the BSA molecules are positively and negatively charged below and above 4.7, respectively (Castro et al. 2009). pzc is significative for interpreting electrostatic interactions between charged materials and molecules. The absorbent possessed positive surface charges due to adsorption of H^+ and/or the protonation below pzc, and negative surface charges owing to adsorption of OH^- and/or the deprotonation

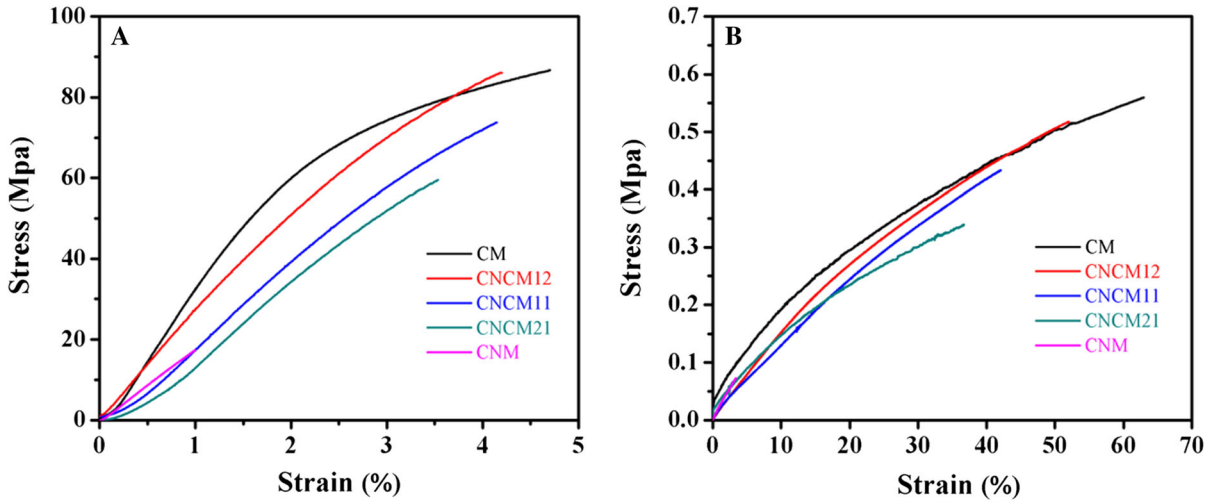

Fig. 4 Stress (σ)/strain (ε) curves of the composite membranes at dry (**A**) and wet (**B**) states

Table 1 The tensile strength and elongation at break of the membranes

Samples	Strength/MPa		Elongation/%	
	Dry	Wet	Dry	Wet
CNM	17.78 ± 1.09	0.07 ± 0.03	0.99 ± 0.07	3.14 ± 0.20
CNCM21	59.72 ± 0.51	0.34 ± 0.04	3.56 ± 0.11	36.58 ± 0.91
CNCM11	73.65 ± 0.62	0.43 ± 0.02	4.07 ± 0.07	42.17 ± 1.36
CNCM12	86.05 ± 0.36	0.50 ± 0.02	4.20 ± 0.07	52.24 ± 0.67
CM	86.72 ± 0.50	0.56 ± 0.02	4.68 ± 0.16	62.74 ± 0.76

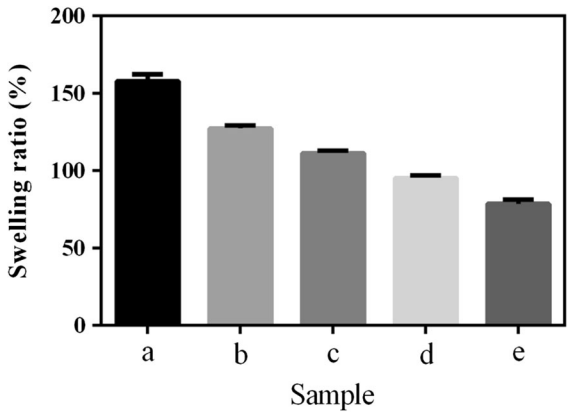

Fig. 5 Swelling behaviors of CNM (a), CNCM21 (b), CNCM11 (c), CNCM12 (d), CM (e)

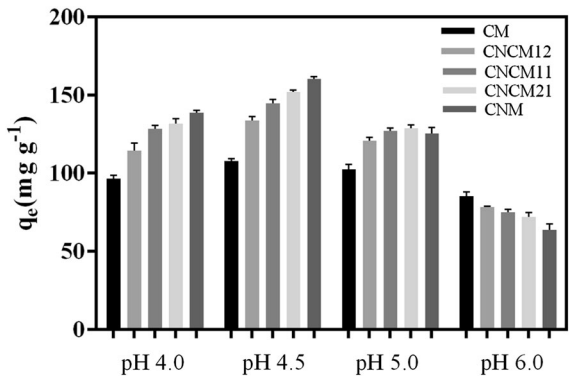

Fig. 6 Effect of pH on BSA adsorption

above pzc (Hubbe et al. 2012; Marek 2014). To better explain the absorption mechanism between the membranes and BSA molecules, the pzc was measured to evaluate the surface charges of the membranes. As shown in Fig. S2, the pzc of the membranes was ~ 2.8. The membranes have positive surface charges due to the protonation of the COO^- groups at pH < 2.8, and negative charges owing to the COO^- groups at pH > 2.8. The maximum BSA adsorption at pH 4.5 for all of the samples was owing to the electrostatic interactions between the composite membranes (negative charged) and BSA molecules

(positive charged). In addition, the composite membranes could absorb more BSA molecules at pH 4.5 than at pH 4.0, and this could be explained by the reason that the composite membranes contain more negative COO^- sites at higher pH above the pzc. The absorption capacities of the composite membranes were decreased when pH increased from 4.5 to 6.0 because of the charge change of the BSA molecules from positive to negative, and the electrostatic interactions between the composite membranes and BSA were altered from attraction to repulsion (Hao et al. 2018). These results indicate that the charges of the composite membranes and BSA molecules at different pH play the dominant role in BSA adsorption.

Adsorption isotherms studies

Based on the above results, CNCM11 was chosen to investigate the adsorption isotherms, and the isotherm data were analyzed by fitting them into various modes to find the available model for this work. It is observed from Fig. 7A that at different temperature (288 K, 298 K, and 308 K), the adsorption amount (q_e) of CNCM11 was significantly increased when the BSA concentration was lower than 1000 mg L^{-1}, and the q_e was then turned to a plateau in the BSA concentration range of 1000–4000 mg L^{-1}. Equilibrium BSA adsorption capacity of 225.3 mg g^{-1}, 235 mg g^{-1}, 241.6 mg g^{-1} were obtained at 288 K, 298 K and 308 K, respectively. To determine the interaction type between CNCM11 and BSA, the BSA adsorption isotherm data was evaluated using Langmuir and Freundlich models (Foo and Hameed 2010; Hlady et al. 1999).

$$\text{Langmuir model:} \quad q_e = \frac{q_m K_L C_e}{1 + K_L C_e} \tag{3}$$

$$\text{Freundlich model:} \quad q_e = k_F C_e^{1/n} \tag{4}$$

where q_m (mg g^{-1}) is the maximum adsorption capacity of the membranes, K_L (L mg^{-1}) is the Langmuir adsorption constant, C_e (mg L^{-1}) is the equilibrium BSA concentration of the solution, k_F (mg g^{-1})(L $mg^{-1})^{1/n}$ is equilibrium adsorption coefficient, and 1/n is an empirical constant. The Langmuir calculation model describes monolayer adsorption on a homogeneous surface with enumerable identical sites, and there is no mutual effect between the adsorbate and no further adsorption occurring, while the Freundlich model is apply to evaluate adsorption on a heterogeneous surface (Tailor et al. 2012).

Nonlinear fitting of the data were summarized in Table 2. Figure 7 compares the theoretical calculation based on adsorption isotherm and experimental data. It was observed from Table 2 that regression coefficient (r^2) obtained from Langmuir model was higher than Freundlich model at all three temperatures, and these results suggest that the adsorption process was better fitted into Langmuir monolayer model (Fu et al. 2016). The dimensionless constant adsorption factor (R_L) of Langmuir model calculated using Eq. (5) (Zhu et al. 2011) is in the range of 0–1, indicating a favorable adsorption of BSA.

$$R_L = \frac{1}{1 + K_L C_0} \tag{5}$$

where K_L (L mg^{-1}) is the Langmuir constant and C_0 is the initial BSA concentration.

Thermodynamic of BSA adsorption

To explore the effect of temperature on BSA adsorption, enthalpy change (ΔH, kJ mol^{-1}), entropy change (ΔS, J K^{-1} mol^{-1}), and standard Gibbs free energy (ΔG, kJ mol^{-1}) were calculated according to equations (Iriarte-Velasco et al. 2011; Juang et al. 2006):

$$K_c = q_m \times K_L \tag{6}$$

$$\ln K_C = -\frac{\Delta H}{RT} + \frac{\Delta S}{R} \tag{7}$$

$$\Delta G = \Delta H - T\Delta S \tag{8}$$

where, K_c (L g^{-1}) is the equilibrium constant, T (K) is the absolute temperature, and R (8.314 J mol^{-1} K^{-1}) is the universal gas constant. ΔH and ΔS obtained from the slope and intercept of linear plot of lnKc versus 1/T (Fig. S3) were summarized in Table S2. The positive ΔH and ΔS suggest the exothermal adsorption process and increased randomness at the membrane-BSA interface, respectively (Sun et al. 2008). The negative ΔG confirmed the thermodynamically favorable and spontaneous adsorption process and the higher ΔG value at higher temperature show more favorable adsorption process (Khattri and Singh 2009).

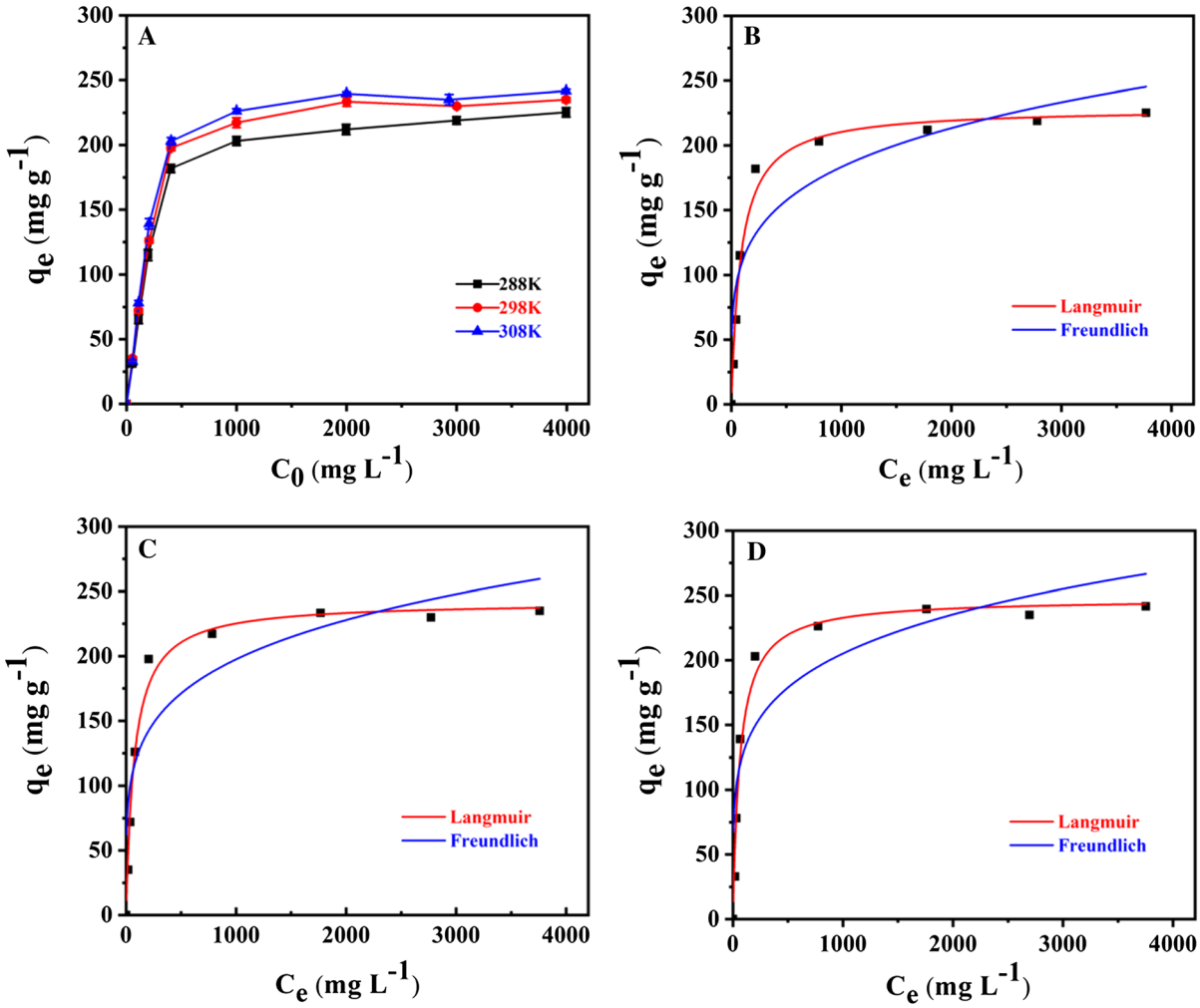

Fig. 7 **(A)** Effect of various initial BSA concentration on adsorption performance; experimental and adsorption isotherm data by Langmuir and Freundlich models at 288 (**B**), 298 (**C**), 308 K (**D**)

Table 2 Isotherm parameters at different temperatures

Isotherm	Parameters	288 K	298 K	308 K
Freundlich	n	4.56	4.84	5.05
	k_F	40.2	47.4	52.2
	r^2	0.8259	0.8133	0.7940
Langmuir	q_m	228.8	242.0	247.6
	K_L	0.0115	0.0134	0.0157
	r^2	0.9814	0.9849	0.9759

Conclusion

In this study, cellulose-based composite membranes were fabricated by a combined dissolution and regeneration of CNF and CF and evaluated as protein adsorbent. The results revealed that the abundant active carboxyl groups of CNF can provide the composite membrane with excellent protein adsorption performance. Meanwhile, the abundant hydroxyl groups in CF and CNF may be helpful for stabilizing the membrane structure due to the intermolecular and intramolecular hydrogen bond formed after the regeneration of CNF and CF. More importantly, the adjustment of CNF/CF ratios can have a direct effect on the mechanical property and adsorption

performance of the composite membranes. These effective and economic composite membranes may have potential application in protein adsorption and can be used in the fields of protein separation and purification.

Acknowledgments This work was supported by the Open Project from Beijing Advanced Innovation Center for Food Nutrition and Human Health, Beijing Technology and Business University (BTBU) (No. 20182013).

References

Abedini R (2011) A novel cellulose acetate (CA) membrane using TiO_2 nanoparticles: preparation, characterization and permeation study. Desalination 277:40–45

Bhatt N, Gupta PK, Naithani S (2011) Hydroxypropyl cellulose from α-cellulose isolated from Lantana camara with respect to DS and rheological behavior. Carbohydr Polym 86:1519–1524

Castro GR, Jingsong C, Bruce P, Kaplan DL (2009) Emulsan-alginate beads for protein adsorption. J Biomater Sci Polym Ed 20:411–426

Chang F, Yamabuki K, Onimura K, Oishi T (2008) Modification of cellulose by using atom transfer radical polymerization and ring-opening polymerization. Polym J 40:1170–1179

Dinand E, Vignon M, Chanzy H, Heux L (2002) Mercerization of primary wall cellulose and its implication for the conversion of cellulose I → cellulose II. Cellulose 9:7–18

Doulabi AH, Mirzadeh H, Imani M, Samadi N (2013) Chitosan/polyethylene glycol fumarate blend film: physical and antibacterial properties. Carbohydr Polym 92:48–56

Duan J, He X, Zhang L (2015) Magnetic cellulose–TiO_2 nanocomposite microspheres for highly selective enrichment of phosphopeptides. Chem Commun 51:338–341

Dubey V, Pandey LK, Saxena C (2005) Pervaporative separation of ethanol/water azeotrope using a novel chitosan-impregnated bacterial cellulose membrane and chitosan-poly(vinyl alcohol) blends. J Membr Sci 251:131–136

Foo KY, Hameed BH (2010) Insights into the modeling of adsorption isotherm systems. Chem Eng J 156:2–10

Fu Q, Wang X, Si Y, Liu L, Yu J, Ding B (2016) Scalable fabrication of electrospun nanofibrous membranes functionalized with citric acid for high-performance protein adsorption. ACS Appl Mater Interfaces 8:11819–11829

Fu LH, Qi C, Liu YJ, Cao WT, Ma MG (2018) Sonochemical synthesis of cellulose/hydroxyapatite nanocomposites and their application in protein adsorption. Sci Rep 8:8292–8303

Handschuh-Wang S, Wang T, Druzhinin SI, Wesner D, Jiang X, Schönherr H (2016) Detailed study of BSA adsorption on micro- and nanocrystalline diamond/β-SiC composite gradient films by time-resolved fluorescence microscopy. Langmuir 33:802–813

Hao W, Chao T, Tian H, Li Y, Wang J (2018) Fabrication of functional magnetic cellulose nanocomposite membranes for controlled adsorption of protein. Cellulose 25:2977–2986

Hazarika P, Behrendt JM, Petersson L, Wingren C, Turner ML (2014) Photopatterning of self assembled monolayers on oxide surfaces for the selective attachment of biomolecules. Biosens Bioelectron 53:82–89

Hlady V, Buijs J, Jennissen HP (1999) Methods for studying protein adsorption. Methods Enzymol 309:402–429

Hu T, Chang C, Zhang L (2011) Efficient adsorption of Hg_{2-} + ions on chitin/cellulose composite membranes prepared via environmentally friendly pathway. Chem Eng J 173:689–697

Hubbe MA, Beck KR, O'Neal WG, Sharma YC (2012) Cellulosic substrates for removal of pollutants from aqueous systems: a review. 2. Dyes. Bioresources 7:2592–2687

Iriarte-Velasco U, Chimeno-AlaníS N, GonzáLez-Marcos MP, Álvarez-Uriarte JI (2011) Relationship between thermodynamic data and adsorption/desorption performance of acid and basic dyes onto activated carbons. J Chem Eng Data 56:2100–2109

Jie C, Lina Z (2006) Unique gelation behavior of cellulose in NaOH/urea aqueous solution. Biomacromol 7:183–189

Juang LC, Wang CC, Lee CK (2006) Adsorption of basic dyes onto MCM-41. Chemosphere 64:1920–1928

Kamide K, Okajima K, Kowsaka K, Matsui T, Nomura S, Hikichi K (1985) Effect of the distribution of substitution of the sodium salt of carboxymethylcellulose on its absorbency toward aqueous liquid. Polym J 17:909–918

Khattri SD, Singh MK (2009) Removal of malachite green from dye wastewater using neem sawdust by adsorption. J Hazard Mater 167:1089–1094

Luan Q et al (2017) Cellulose-based composite macrogels from cellulose fiber and cellulose nanofiber as intestine delivery vehicles for probiotics. J Agric Food Chem 66:339–345

Luo X, Liu S, Zhou J, Zhang L (2009) In situ synthesis of Fe_3O_4/cellulose microspheres with magnetic-induced protein delivery. J Mater Chem 19:3538–3545

Madaeni SS, Heidary F (2011) Improving separation capability of regenerated cellulose ultrafiltration membrane by surface modification. Appl Surf Sci 257:4870–4876

Marek K (2014) The pH dependent surface charging and points of zero charge. VI. Update. J Colloid Interface Sci 426:209–212

Meng H, Chang C, Na P, Zhang L (2012) Structure and properties of hydroxyapatite/cellulose nanocomposite films. Carbohydr Polym 87:2512–2518

Montanari S, Roumani M, Laurent Heux A, Vignon MR (2008) Topochemistry of carboxylated cellulose nanocrystals resulting from TEMPO-mediated oxidation. Macromolecules 38:1665–1671

Pelton R (2009) Bioactive paper provides a low-cost platform for diagnostics. TrAC Trends Anal Chem 28:925–942

Richter AG, Ivan K (2013) Using in situ X-ray reflectivity to study protein adsorption on hydrophilic and hydrophobic surfaces: benefits and limitations. Langmuir 29:5167–5180

Sadir S, Prabhakaran MP, Wicaksono DHB, Ramakrishna S (2014) Fiber based enzyme-linked immunosorbent assay for C-reactive protein. Sensors Actuators B Chem 205:50–60

Sahadevan R, Crandall C, Schneiderman S, Menkhaus TJ (2018) Cellulose-graft-polyethyleneamidoamine anion-

exchange nanofiber membranes for simultaneous protein adsorption and virus filtration. ACS Appl Nano Mater 1:3321–3330

Sang YO et al (2005) Crystalline structure analysis of cellulose treated with sodium hydroxide and carbon dioxide by means of X-ray diffraction and FTIR spectroscopy. Carbohydr Res 340:2376–2391

Sun XF, Wang SG, Liu XW, Gong WX, Bao N, Gao BY, Zhang HY (2008) Biosorption of Malachite Green from aqueous solutions onto aerobic granules: kinetic and equilibrium studies. Biores Technol 99:3475–3483

Tailor R, Shah BA, Shah AV (2012) Sorptive removal of phenol by zeolitic bagasse fly ash: equilibrium, kinetics, and column studies. J Chem Eng Data 57:1437–1448

Tsuguyuki S, Satoshi K, Yoshiharu N, Akira I (2007) Cellulose nanofibers prepared by TEMPO-mediated oxidation of native cellulose. Biomacromol 8:2485–2491

Udoetok IA, Dimmick RM, Wilson LD, Headley JV (2016) Adsorption properties of cross-linked cellulose-epichlorohydrin polymers in aqueous solution. Carbohydr Polym 136:329–340

Yang F, Wang J, Hou J, Guo H, Liu C (2013) Bone regeneration using cell-mediated responsive degradable PEG-based scaffolds incorporating with rhBMP-2. Biomaterials 34:1514–1528

Zhang H et al (2017) Cellulose anionic hydrogels based on cellulose nanofibers as natural stimulants for seed germination and seedling growth. J Agric Food Chem 65:3785–3791

Zhang H et al (2018) A pH-responsive gel macrosphere based on sodium alginate and cellulose nanofiber for potential intestinal delivery of probiotics. ACS Sustain Chem Eng 6:13924–13931

Zhao ZP, Wang Z, Wang SC (2003) Formation, charged characteristic and BSA adsorption behavior of carboxymethyl chitosan/PES composite MF membrane. J Membr Sci 217:151–158

Zhu B, Nan M, Wu D, Sun Y, Li W (2011) Synergistic extraction and selective removal of Cu^{2+} from aqueous solution using magnetic nanoparticles coated with mixtures of sodium oleate and saponified 2-ethylhexyl phosphonic acid mono-2-ethylhexyl ester. Ind Eng Chem Res 50:11698–11705